Monte Carlo Simulation of Leading Order Top Quark Production

Candidate Number: 8276S

May 11, 2015

Abstract

The aim of the project was to produce a simulation of leading order top quark production. Using a Monte Carlo integration, the program calculates the differential cross section at a given energy without spin averaging the top quark pair. Initial results were shown to be in agreement with comparable programs. The results show the quark channel cross section higher at energies below $1300GeV$, whereas at LHC energies the gluon channel dominates. At $1600GeV$, peaks in the cross section were found at 0 rapidity, $\sim 350GeV$ centre of mass energy, and approximately $80GeV$ transverse momentum.

Contents

1 Introduction

The Standard Model (SM) explains how the fundamental particles that make up matter in the universe interact, and successfully describes a huge range of diverse phenomena. Since the current formulation was finalised in the 1970s it has been relentlessly tested, with experiments consistently confirming the theory. However, with the completion of the Large Hadron Collider (LHC), experiments can be done to test the SM at higher energies than ever before, and could potentially find new physics. [1]

The top quark was predicted, along with the bottom quark, in 1973, by Makoto Kobayashi and Toshihide Maskawa, as a means of explaining CP violations in kaon decays.[2] However, it wasn't until 1995 that the top was finally discovered.[3] This is because its mass $m_t = 173.2 \pm 0.9 GeV$, around 40 times heavier than the next heaviest quark, the bottom.[4] This makes it the heaviest fundamental particle in the standard model, and thus uniquely interesting to study.

1.1 Motivation

The top quark has a Yukawa coupling to the Higgs boson of order unity, far higher than any other quark. This suggests it may play a special role in discovering new physics beyond the Standard Model, and motivates questions such as 'Why is the top quark so much heavier than the other quarks?' 'Are there undiscovered particles the top quark can decay into?' Some super-symmetry

models theorise this. The interplay between the Higgs boson and the top quark is also the key to understanding whether the recently discovered Higgs boson is the SM Higgs, or another Higgs as predicted by Beyond Standard Model (BSM) theories. It can also be used to probe mechanisms that break electroweak gauge symmetry, which could lead to further understanding of this force.[5] [6]

Another important property of the top quark is its very short predicted lifetime, $\tau \approx 5 \times 10^{-25} s$.[4] This is approximately 10 times shorter than the time taken for hadronisation, meaning the top quark provides a unique opportunity to study bare quark interaction.[3] [5]

To answer these questions, an understanding of the creation and decay of top quarks is essential. At the LHC, about 8 million top anti-top ($t\bar{t}$) pairs can be produced per experiment per year, and accurate simulations are needed to predict the decays.[7] This project attempts to produce these simulations, so they can be used in further research.

1.2 Overview

The program I have created uses Monte Carlo integration to calculate the differential cross section for top pair production at leading order. The results are sorted into bins, which can then be plotted to give histograms. The program does not average over the $t\bar{t}$ spins, making it easy to extend this program to include fully differential decay. This could then be used to test against experimental data from the LHC.

In this paper I will firstly give a brief outline of the theory behind top pair production and the program itself. In Section 4, I will explain some of the checks done to ensure the program is working correctly, before discussing some results obtained using the program. Finally, I will suggest some improvements and extensions to the program that could be made in the future. All numerical values given throughout the paper are in natural units, $\hbar = c = 1$.

2 Theory

The basic idea of the program is to replicate collisions in the LHC. There are two beams of protons fired at each other, each with energy P. (The program may also be used to simulate $p\bar{p}$ collisions, but the theory is the same). Because of the high energies involved, $t\bar{t}$ pairs are produced via deep inelastic scattering collisions between the fundamental particles within the protons, the partons, whose masses can be neglected. [8] Their energies will therefore be of the form $x_i P$, where x_i are the fractions of energies carried by the partons, $0 < x_i \leq 1$.

To easily link production to decay, and so for this program to be of any use, a crucial approximation must be made, the narrow width approximation. Once

produced, the $t\bar{t}$ pair decay, meaning they should be treated as propagators within one Feynman diagram including both production and decay. The narrow width approximation assumes they are on shell, so the production and decay cross sections can be treated separately, and simply convolved together. This is a valid assumption, making it easy to extend the program. [5] [9]

2.1 Kinematics

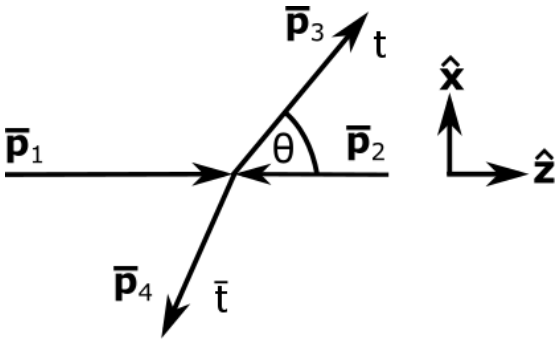

Figure 1: Two proton beams, with momenta $\bar{p}_1$ and $\bar{p}_2$, collide to produce a top and anti-top, of momenta $\bar{p}_3$ and $\bar{p}_4$ respectively. Here θ is the angle between the outgoing top quark and the z-axis.

The kinematics of the collision can be calculated using conservation of four-momenta, and in the lab frame yield the following results, with the variables as defined in Figure 1:

$$\mathbf{p}_1 = (x_1 P, 0, 0, x_1 P) \tag{1}$$

$$\mathbf{p}_2 = (x_2 P, 0, 0, -x_2 P) \tag{2}$$

$$\mathbf{p}_3 = (\sqrt{|\bar{p}_3^2| + m^2}, |\bar{p}_3| \sin(\theta), 0, |\bar{p}_3| \cos(\theta)) \tag{3}$$

$$\mathbf{p}_4 = ((x_1 + x_2)P - \sqrt{|\bar{p}_3^2| + m^2}, -|\bar{p}_3| \sin(\theta), 0, (x_1 - x_2)P - |\bar{p}_3| \cos(\theta)) \tag{4}$$

Where without loss of generality the y components have been set to zero. Using the energy equation $E_4^2 = |\bar{p}_4|^2 + m^2$, it can be shown that:

$$p_3 = \frac{2Px_1x_2\cos(\theta)(x_1 - x_2) + (x_1 + x_2)\sqrt{(2Px_1x_2)^2 + (m(x_1 - x_2)\cos(\theta))^2 - (m(x_1 + x_2))^2}}{(x_1 + x_2)^2 - (x_1 - x_2)^2\cos^2(\theta)} \tag{5}$$

Using these results, the kinematics of a collision are fully specified by the two ingoing momenta and the angle of the outgoing top quark to the z-axis.

2.2 Cross-section

The fully differential cross section to be calculated is:

$$d\sigma = \sum_{ij} \left|M_{ij}^2\right| pdf_i(x_1, Q^2) pdf_j(x_2, Q^2) d\Phi dx_1 dx_2 \tag{6}$$

where the indices i and j represent the partons in the proton. $pdf_i(x_k, Q^2)$ is the parton distribution function (PDF), a probability distribution of the parton i in the proton. $\left|M_{ij}^2\right|$ is the matrix element, Q is the factorisation scale that the PDF is evaluated at, and $d\Phi$ is the phase space.

In the lab frame, this phase space can be written as:

$$d\Phi = \left(\frac{1}{128\pi^2 x_1 x_2 P^3}\right) \frac{\left|\bar{p}_3^2\right|}{|\bar{p}_3|\,(x_1 + x_2) + (x_2 - x_1) E_3 \cos(\theta)} d\Omega \tag{7}$$

where $d\Omega$ is the solid angle element in the lab frame, and E_3 is the energy of particle 3.

2.3 Matrix Elements

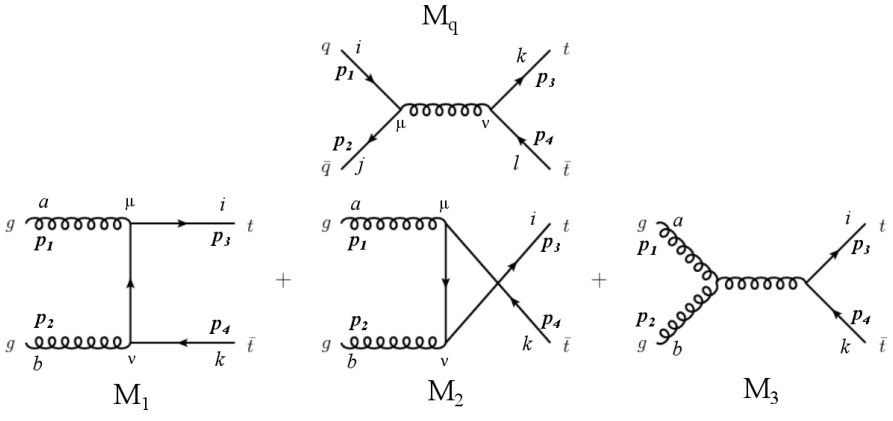

Figure 2: Feynman diagrams for leading order top pair production. M_q is a $q\bar{q}$ collision, and M_1, M_2 and M_3 are gg collisions. The colour indices are denoted by Latin letters, the Lorentz indices by Greek.[10]

At leading order there are four Feynman diagrams, shown in Figure 2, which result in the following matrix elements:

$$M_q = -\frac{g^2}{(\mathbf{p}_1+\mathbf{p}_2)^2}\bar{v}(\mathbf{p}_2)\gamma^\mu u(\mathbf{p}_1)\bar{u}(\mathbf{p}_3)\gamma_\mu v(\mathbf{p}_4)T_a{}^i_j T^a{}^k_l \tag{8}$$

$$M_1 = -\frac{g^2}{2(\mathbf{p}_1\cdot\mathbf{p}_3)}\bar{u}(\mathbf{p}_3)\gamma^\mu(\not{p}_3-\not{p}_1+m)\gamma^\nu v(\mathbf{p}_4)\epsilon_\mu(\mathbf{p}_1)\epsilon_\nu(\mathbf{p}_2)T_a{}^i_j T^b{}^j_k \tag{9}$$

$$M_2 = -\frac{g^2}{2(\mathbf{p}_2\cdot\mathbf{p}_3)}\bar{u}(\mathbf{p}_3)\gamma^\nu(\not{p}_3-\not{p}_2+m)\gamma^\mu v(\mathbf{p}_4)\epsilon_\mu(\mathbf{p}_1)\epsilon_\nu(\mathbf{p}_2)T_b{}^i_j T^a{}^j_k \tag{10}$$

$$\begin{aligned} M_3 = \frac{ig^2}{(\mathbf{p}_1+\mathbf{p}_2)^2}&\bar{u}(\mathbf{p}_3)\gamma^\rho v(\mathbf{p}_4)\epsilon_\mu(\mathbf{p}_1)\epsilon_\nu(\mathbf{p}_2) \\ &[(\mathbf{p}_1-\mathbf{p}_2)_\rho g_{\mu\nu}+(2\mathbf{p}_2+\mathbf{p}_1)_\mu g_{\nu\rho}-(2\mathbf{p}_1+\mathbf{p}_2)_\nu g_{\mu\rho})]T_c{}^i_k f^{abc} \end{aligned} \tag{11}$$

where g is related to the coupling constant, $g^2 = 4\pi\alpha_s$, $\epsilon_\mu(\mathbf{p})$ are the polarisation vectors of the gluons, and the $T^a{}^j_k$ terms at the end are the colour factors, which will be explained in the following section. Spin indices have been suppressed for clarity.

These matrix elements can then be squared and used in the cross section described above. The incoming particles' spins and polarisations can be averaged over using standard spin sum rules. However, I don't want to average over the $t\bar{t}$ spins, so I use the relations:

$$u(p_i)\bar{u}(p_i) = (\not{p}_i + m_i)(1+\gamma^5\not{s}_i) \tag{12}$$

$$v(p_i)\bar{v}(p_i) = (\not{p}_i - m_i)(1+\gamma^5\not{s}_i) \tag{13}$$

where $\mathbf{s}$ is the spin four-vector:

$$\mathbf{s}_\pm = \pm\left(\frac{|\bar{p}|}{m}, \frac{E}{m}\frac{\bar{\mathbf{p}}}{|\bar{p}|}\right) \tag{14}$$

Here the $\pm$ states correspond to the positive/negative helicity eigenstates. In the program, the helicities of t and $\bar{t}$ are represented by variables j_3 and j_4, with these taking values of ± 1.[11]

Because there are three diagrams for gluon-gluon events, when squaring the matrix element these can interfere, giving the result:

$$|M_1+M_2+M_3|^2 = |M_1|^2+|M_2|^2+|M_3|^2+2\Re(M_1M_2^*+M_1M_3^*+M_2M_3^*) \tag{15}$$

The coupling constant, α_s and the parton distribution functions depend on the energy scale, Q. I will be evaluating both at m_{top} (ie. the factorisation and normalisation scales are both set to m_{top}). This is in line with Top++, a program I have used for comparison. [12]

2.4 Colour Factors

The $T^{a\,j}_{\ k}$ terms in the matrix elements are the generators of $SU(3)$, which represents colour. To obtain the cross section the colours have to be averaged over, giving the following results (for derivations see Appendix 8.1):

$$C_{M_q^2} = \frac{2}{9}, \quad C_{M_1^2} = \frac{1}{12}, \quad C_{M_2^2} = \frac{1}{12}, \quad C_{M_3^2} = \frac{3}{16}$$

$$C_{M_1 M_2^*} = -\frac{1}{96} \quad C_{M_1 M_3^*} = \frac{3i}{32} \quad C_{M_2 M_3^*} = -\frac{3i}{32}$$

2.5 Other Diagrams

Some thought needs to be given to other methods of producing top quarks. As well as the aforementioned diagrams, there is also a single top production method. However, this can be distinguished from $t\bar{t}$ production in experiments, so doesn't need to be included. [13] Top pairs could also be produced via electroweak interactions, however these corrections are small when compared to errors assosciated with the PDFs or higher order corrections, so aren't considered. [14]

3 Program

The program employs a Monte Carlo routine to integrate over the partonic variables x_1 and x_2, and outputs histograms showing the relation between cross section and various other variables. No knowledge of programming is required to use it, as all the parameters can be altered from a config file, *param.cfg*. To start the program, run *TopPro*.

3.1 Prerequisites

These libraries must be installed before using the program:

- LHAPDF5.9.1: https://lhapdf.hepforge.org/
  The Les Houches Accord Parton Distribution Functions is a library which calculates PDF and coupling constant values. This should be installed in /usr along with a PDF set, which has to be downloaded separately. Throughout this paper, results and tests were run using the PDF set NNPDF3.0 unless otherwise stated.[15]

- GNU: http://www.gnu.org/software/gsl/gsl.html
  GNU Scientific Library (GSL) is required for the random number generation.

- libConfig: http://www.hyperrealm.com/libconfig/
  A library used for the config file.

3.2 How to Use

The following list explains the options available in *param.cfg*:

- TMass: The mass of the top quark.
- ColliderType: Set to -1 for a $p\bar{p}$ collider or $+1$ for a pp collider. The default is for pp.
- BeamEnergy: Energy of each proton beam in GeV.
- PDFName: Name of the PDF used. New PDFs can be downloaded using the LHAPDF interface. Uses NNPDF30_lo_as_0118.LHgrid by default.
- N: Number of events. Higher N will lead to more accurate results, but will take longer. The default is 10^6.
- Pol: Set to 0 to average over the $t\bar{t}$ spins, or 1 to keep specific helicities.

There are also options for each histogram:

- min: The lower limit on the histogram.
- max: The upper limit on the histogram.
- bins: The number of bins in the histogram.

There is a backup file, *parambac.cfg* which can restore the config file to its default parameters.

3.3 How it Works

For more major changes the code itself may need to be altered. Here I give a brief explanation of how the program works, to aid in editing it.

The file *mc.cc* contains the Monte Carlo routine. Random numbers are assigned to x_1, x_2 and θ, with $x_{min} < x_i < 1$ and $0 < \theta < \pi$. The lower limits on the parton fractions, x_{min}, are set as the lowest value for which the PDFs are defined. A reliable random number generator is crucial for a Monte Carlo integration. The GSL has passed the 'Diehard Statistical Tests' for random number generation, so will create an unbiased distribution. [16] The helicities of the top pair are set to ± 1, after which the program checks if, given these initial conditions, the $t\bar{t}$ production is kinematically allowed. If so, the four-momenta and cross section of the event are calculated using the results given above, with the actual matrix elements stored in *qqmatrix.hh* and *ggmatrix.hh*. Results are stored in the file *results.txt*. Each row in the file represents an event, with the ten columns being:

$$x_1,\ x_2,\ \theta,\ j_3,\ j_4,\ |\bar{p}_3|,\ E_3,\ E_4,\ |\bar{p}_4|,\ d\sigma$$

The histogram function in *histogram.hh* creates histograms from the event data in *results.txt*. It produces histograms of the differential cross section vs rapidity, centre of mass energy, and transverse momentum by default, though others could easily be added. If an event falls outside the limits set in *param.cfg* it is discarded. If an event is exactly on the boundary between two bins it is put in the upper bin, although this is very unlikely given the variables are assigned as doubles. The resulting histogram data is stored in *hist.txt*. The first three columns are for rapidity, the second three for centre of mass energy, and the final three correspond to transverse momentum. The three columns within each histogram represent bin value, cross section/pb, and error in cross section/pb. The bin value is the central value of the bin.

This data can then be turned into a histogram plot using a program of the user's choice. For my results I have used Gnuplot 4.6.5. Finally, the program outputs the total cross section and assosciated error.

3.4 Errors

The great benefit of Monte Carlo integration is that the error falls as $1/\sqrt{N}$ regardless of the number of dimensions. An estimation of the error given by Monte Carlo integration is: [17]

$$Error = \pm V \sqrt{\frac{\langle f^2 \rangle - \langle f \rangle^2}{N}} \tag{16}$$

where

$$\langle f \rangle = \frac{1}{N} \sum_{i=1}^{N} f(x_i) \tag{17}$$

$$\langle f^2 \rangle = \frac{1}{N} \sum_{i=1}^{N} f^2(x_i) \tag{18}$$

This is the error the program returns after a single run, and is how the errors in the histograms are calculated. However, this isn't guaranteed to be a good error estimate, as it is not Gaussian distributed. [16] A more reliable error can be found by running the program several times, and using the standard deviation of these results.

Aside from the Monte Carlo, another important source of error is the LHAPDF. The PDFs and coupling constant have errors assosciated with them, which are given by functions within LHAPDF. These are calculated by averaging over the 100 PDF sets stored within each PDF, and at a factorisation scale of m_t gives errors of about 10% for individual events. These slow down the convergence of the integration, however over enough iterations they will be averaged out. The accuracy of doubles stored in C++ is ~ 16 significant figures, rendering errors associated with these negligible. [18]

4 Checks

It is very important not to just have the program running, but to know it is doing what it should be doing. Each section of the program has been checked individually, to ensure it is running correctly.

4.1 Monte Carlo

To check the Monte Carlo simulation was working, I ran it with a simple analytically integrable function in place of the cross section:

$$\sigma = \int_0^{\pi} (\sin^2(\theta) + \theta^2 + \theta) d\theta$$

Analytically, the result is:

$$\sigma = \frac{\pi}{2} + \frac{\pi^3}{3} + \frac{\pi^2}{2} = 16.841$$

Running the program with $N = 10^6$ gave 16.85 ± 0.04, which agrees within errors.

4.2 Parton Distribution Function Checks

To check the PDFs were giving the correct values, and that LHAPDF was installed correctly, I checked some integrals that give analytical results:

$$\sigma = \int_0^1 (u(x) - \bar{u}(x)) dx = 2 \tag{19}$$

$$\sigma = \int_0^1 (d(x) - \bar{d}(x)) dx = 1 \tag{20}$$

$$\sigma = \int_0^1 (s(x) - \bar{s}(x)) dx = 0 \tag{21}$$

$$\sigma = \int_0^1 (\sum_{i=1}^{5} (q_i(x) + \bar{q_i}(x) + g(x))x) dx = 1 \tag{22}$$

where u, d, s, g represent the PDFs for the up, down and strange quark, and gluon respectively. These results use the difference between quark and anti-quark distributions to calculate the number of valence quarks in the proton. [19] Integrating the PDF functions from LHAPDF with $N = 10^6$ gives:

(19) 1.98 ± 0.02
(20) 0.979 ± 0.007
(21) -0.001 ± 0.003
(22) 1.019 ± 0.005

Although these aren't all within error, as previously mentioned the Monte Carlo error isn't completely accurate. Running five times and calculating the standard deviation gives 1.00 ± 0.04 for (20), and 1.01 ± 0.01 for (22), correct within errors and suggesting the PDF functions are returning the correct values.

4.3 Matrix Element

To square the matrix elements I used trace techniques combined with Mathematica (see Appendix 8.2 for details). To check the amplitudes were being squared correctly I calculated the spin-averaged versions, for example for the $q\bar{q}$ channel this is:

$$M_{qq}^2 = \frac{4g^4}{9(\mathbf{p}_1 \cdot \mathbf{p}_2)^2}((\mathbf{p}_1 \cdot \mathbf{p}_2)(\mathbf{p}_2 \cdot \mathbf{p}_4) + (\mathbf{p}_2 \cdot \mathbf{p}_3)(\mathbf{p}_1 \cdot \mathbf{p}_4) + m^2(\mathbf{p}_1 \cdot \mathbf{p}_2)) \quad (23)$$

These were then compared with my results for $j_3 = j_4 = 0$, and gave exactly the same values, confirming my matrix elements as correct.

4.4 Kinematics

To check the kinematics ($\mathbf{p}_3$, $\mathbf{p}_4$) were correct , I compared them with the program MadGraph 5. [20] MadGraph also calculates cross sections for collisions, so generating the $t\bar{t}$ process gave some results I could compare with. Choosing specific values of x_1, x_2 and θ and looking at the kinematic results showed they are in agreement.

4.5 Further Checks

The total cross section excluding the PDFs was compared to results given in [21]. This paper gives the analytical cross section for specific values of x_1 and x_2, excluding the PDFs, so essentially setting them equal to delta functions:

$$\hat{\sigma}_{ij}|_{x_1,x_2} = \int \left|M_{ij}^2\right| d\Phi \quad (24)$$

Testing this with several values of x_1 and x_2 shows an agreement with the total cross section I calculate numerically.

4.6 Performance

Because the program relies on a large number of iterations for accuracy, efficient code is vital. I have cut down the run time in various ways, for instance only calculating the kinematics if a collision is allowed, and if possible avoiding calculating the same quantity twice. For $N = 10^5$ a typical run takes $\sim 60s$. Of this $60s$, $43s$ is spent intialising LHAPDF and obtaining the PDF values. Clearly, to improve the speed either LHAPDF needs to be sped up, or a method needs to be used which requires less iterations (see Section 6).

5 Results and Analysis

In this section I outline some results obtained using the program. All calculations use $m_t = 173.3GeV$, in line with the Top++ default. The PDF used was the NNPDF3.0 NF=5 lowest order grid.

5.1 Total Cross Sections

Beam Energy/GeV	Cross Section/pb	
	Top++	My Program
400	0.00442	0.00440±0.00005
800	0.460	0.462±0.003
1600	9.15	9.12±0.03
3200	83	83±3
6500	507	509±4

Table 1: Total cross section results for different beam energies, compared against Top++ at leading order. The results were obtained by averaging 10 runs of $N = 10^6$ iterations.

Beam Energy/GeV	Cross Section/pb			
	gg channel		$q\bar{q}$ channel	
	Top++	My Program	Top++	My Program
400	7.388×10^{-5}	$(7.381\pm0.013)\times10^{-5}$	0.00433798	0.004328±0.00005
800	0.106984	0.1071±0.0002	0.353389	0.355±0.003
1600	4.8907	4.89±0.03	4.26112	4.26±0.03
3200	62.8089	64±3	20.0362	19.8±0.3
6500	443.896	438±5	63.2379	63±2

Table 2: Cross section results for the separate partonic channels. Averaged over 10 runs at $N = 10^6$, with Top++ results at leading order for comparison.

Table 1 shows the total cross sections for various beam energies, with a comparison to Top++. Table 2 is similar, but with the cross section broken down into the separate $q\bar{q}$ and gg contributions. In both cases the results are in agreement. Plotting the cross sections for $q\bar{q}$ and gg channels against beam energy gives the graph in Figure 3. At low energies the $q\bar{q}$ cross section dominates, but at $\sim 1300GeV$ the two lines cross over, and above this energy the gg cross section is higher. At LHC energies of $6500GeV$, the gluon channel makes up approximately 90% of the cross section. This can be explained by looking at the forms of the PDFs, shown in Figure 4. At lower energies, the average parton momentum fractions have to be higher for the process to be kinematically allowed. Quark PDFs are higher at larger momentum fractions, so the $q\bar{q}$ process dominates. At larger beam energies the average momentum fractions are lower,

so the gluon PDFs are favoured. [22]

I also ran the program with the spins of the $t\bar{t}$ pair correlated, $j_3 = j_4$, and anti-correlated, $j_3 = -j_4$. The cross section was higher for the correlated spins than for the anti-correlated, with cross sections of $\sigma = (586 \pm 5)pb$ and $\sigma = (433 \pm 5)pb$ respectively at $6500GeV$.

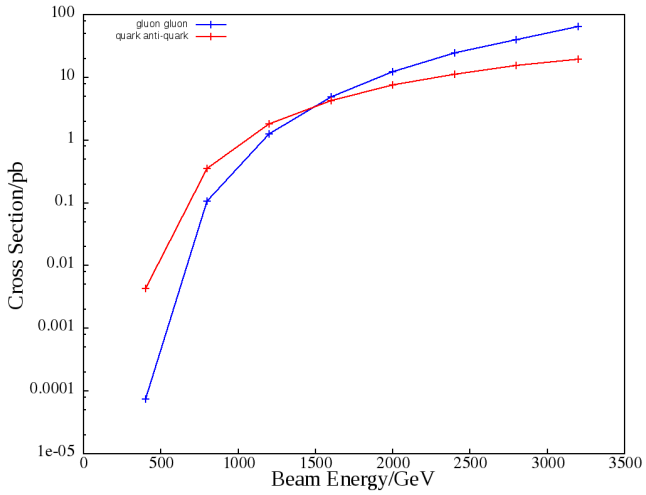

Figure 3: Cross section against beam energy for the gg and $q\bar{q}$ partonic channels, run with $N = 10^6$. Note the log scale on the y-axis.

5.2 Differential Cross Sections

Using Gnuplot4.6.5, graphs were made of the differential cross sections. Figures 5-7 show histograms of the rapidity, centre of mass energy and transverse momentum at $P = 1600GeV$, from my program and MadGraph. The errors are small, particularly on Figures 6 and 7, where the error bars are barely visible. $N = 10^7$ is clearly a sufficient amount of iterations at this energy and number of bins. The graphs from my program and MadGraph are of similar shapes and sizes, another indication that the program is behaving correctly. Figure 5 shows a peak in the cross section when the rapidity is zero, showing the cross section is highest for events for which the top quark momentum is perpendicular to that of the proton beam. The peak given by my program is at $0.77pb$, slightly below that of the MadGraph plot. This could be due to errors in the data (MadGraph doesn't give errors for the histograms), but more investigation is needed to be certain. From Figure 6 it is clear that the cross section is zero below a centre of mass energy of $\sim 350GeV$. This is to be expected, given that for the collision to occur $E_{CoM} \geq 2m_t$. The peak of the graph is at this threshold energy, with the cross section becoming smaller with increasing centre of mass energy beyond

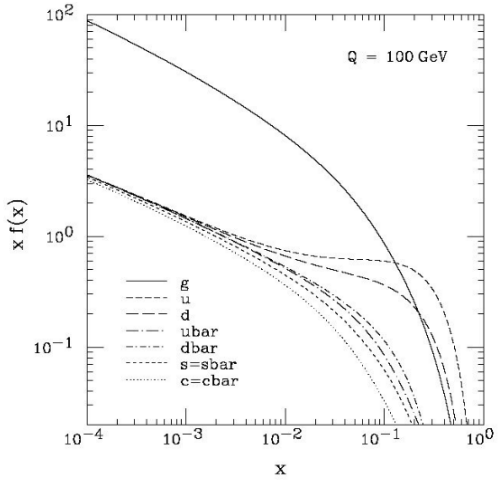

Figure 4: Example PDFs, evaluated at a factorisation scale of $Q = 100GeV$. The curves are multiplied by x to better illustrate the behaviour at both ends.[23]

this. Figure 7 shows the cross section for transverse momentum increasing to a peak at approximately $80GeV$, then decaying at energies above this.

Figure 8 compares graphs of cross section against transverse momentum for two different collider energies, $1600GeV$ and $6500GeV$. The total cross section changes, however the shape of the graph remains the same, with a peak cross section at $\sim 80GeV$. Further study could show if this shape is scale invariant.

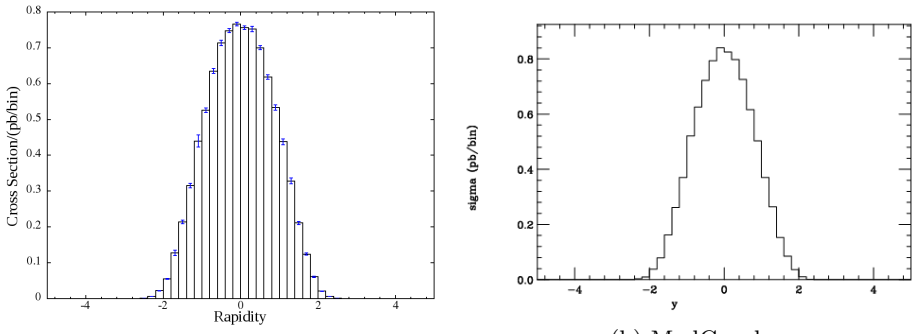

(a) My Program

(b) MadGraph

Figure 5: Comparison of rapidity against cross section for my program and MadGraph. Run at $P = 1600GeV$ with $N = 10^7$. No errors were available for the MadGraph data.

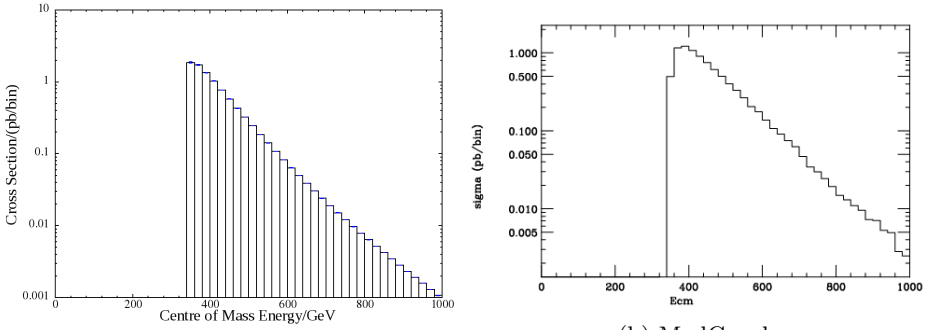

(a) My Program

(b) MadGraph

Figure 6: Comparison of centre of mass energy against cross section for my program and MadGraph. Run at $P = 1600GeV$ with $N = 10^7$. No errors were available for the MadGraph data. Note the log scale on the y-axis.

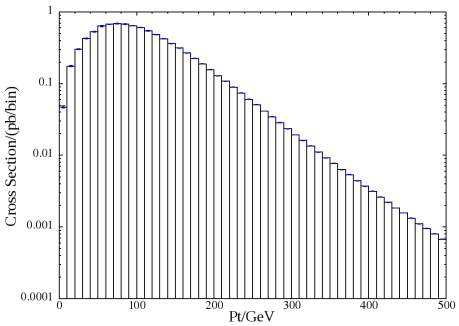

(a) My Program

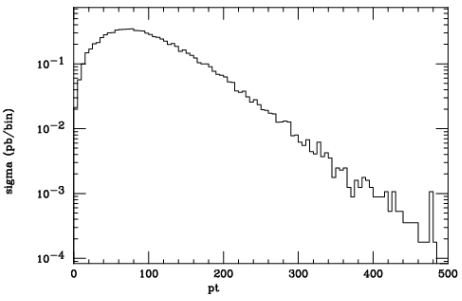

(b) MadGraph

Figure 7: Comparison of transverse momentum against cross section for my program and MadGraph. Run at $P = 1600GeV$ with $N = 10^7$. No errors were available for the MadGraph data. Note the log scale on the y-axis.

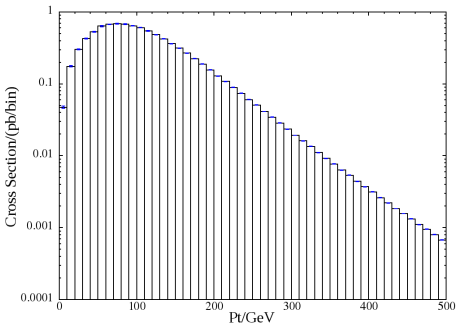

(a) $P = 1600GeV$

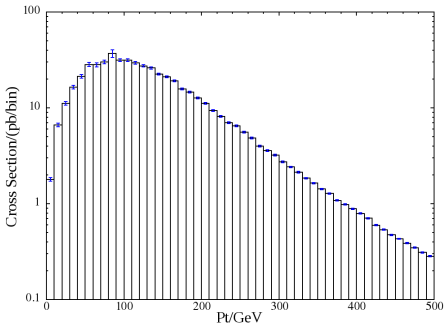

(b) P=6500GeV

Figure 8: Comparison of transverse momentum against cross section for different beam energies. Run with $N = 10^7$.

6 Further Improvements

Working on this project I ran into quite a few unforseen problems, meaning I didn't achieve all the aims I originally set out. Given more time, various things could be done to extend and enhance the program.

6.1 More Analysis

I only had a few days to analyse the results, so haven't tested the program with a wide range of input parameters. Although the program seems to be functioning correctly, more checks of the differential cross sections are needed to confirm this. Further investigations could also look quantatively into how the shapes of the graphs change with different beam energies. Fixed order results have a residual dependence on factorisation and renormalisation scales, so examining the results when changing these could prove insightful. [22] Another interesting experiment would be to compare the distributions for the cases where the $t\bar{t}$ spins are correlated/anti-correlated, to see if there is a notable difference.

6.2 Adaptive Monte Carlo

An adaptive Monte Carlo takes more samples where the integrand is larger, dividing the integration hypervolume into subregions. This can speed up calculation time and reduce the error. A comparison between the plain Monte Carlo integration used here and an adaptive algorithm, the VEGAS algorithm, give errors of 0.01 vs 0.0003 for the same number of samples. This would make high accuracy calculations much more feasible. [24]

6.3 Improving the Program

Aside from changing the Monte Carlo method, there are other ways the program could be improved. More customisability could be added to the *param.cfg* file, for instance options to change the factorisation and renormalisation scales, or the ability to add different histograms. Cutoff options would help to compare the results with real data.

6.4 Decay

Because of the narrow width approximation, including the leading order $t\bar{t}$ decays would be simple. The top decays almost entirely via the $t \to W^+b$ channel, as implied by the CKM matrix.[25] The W-boson can then decay into either leptons or a quark and anti-quark, as shown in Figure 10. These are the particles detected in collisions at the LHC, as either leptons or jets. Once decay is included the results can be compared with real data.

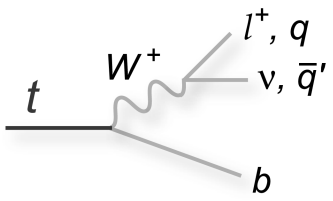

Figure 9: The dominant decay mode of the top quark at leading order. The W-boson can decay into leptons or quarks.

6.5 Higher Orders

This program only includes the leading order contribution to the cross section, limiting its use for high accuracy comparisons with real data. Next-to-next-to leading order contributions have been shown to increase the cross section by approximately 30%. [22] They would also allow the investigation of interesting phenomena not seen at leading order, such as charge asymmetry. [27]Including these would be the next step in improving the program, with programs such as NNTopDec and Top++ being potentially useful.[26] [12]

7 Conclusion

In conclusion, the program calculates the differential cross section of $t\bar{t}$ production at leading order, without averaging over helicities. The results produced are in agreement with other cross section calculation programs, a good indication that they are accurate, though more analysis needs to be done to be sure. They show the $q\bar{q}$ channel cross section is higher at energies below $1300GeV$, but at high energies such as those achieved at the LHC the gg channel is dominant. Cross sections were found to be higher when the $t\bar{t}$ spins were correlated as opposed to anti-correlated, with values of $\sigma = (586 \pm 5)pb$ and $\sigma = (433 \pm 5)pb$ respectively at $6500GeV$. At $1600GeV$ the histograms produced show peaks in the cross section at zero rapidity, a centre of mass energy of $\sim 350GeV$, and a transverse momentum of approximately $80GeV$. Further research could be done to include higher order production and decay contributions in the program, allowing it to be more accurate in predicting experimental results.

References

[1] http://en.wikipedia.org/wiki/Standard_Model

[2] M. Kobayashi, T. Maskawa (1973). "CP-Violation in the Renormalizable Theory of Weak Interaction". Progress of Theoretical Physics 49

[3] Frank-Peter Schilling (2012). "Top Quark Physics at the LHC" Institute of Experimental Nuclear Physics (EKP) arXiv1206.4484

[4] PDG Top Quark Review 2013 http://pdg.lbl.gov/2013/reviews/rpp2013-rev-top-quark.pdf

[5] Martin Gorner "Differential Cross Sections for Top Quark Pair Production in the e/μ Jets Final State at $\sqrt{s} = 8TeV$ in CMS" Hamburg University (2014)

[6] John Freeman "A Measurement of the Top Quark Mass in 1.96TeV $p\bar{p}$ Collisions Using a Novel Matrix Element Method" University of California (2007)

[7] M. Beneke, I. Efthymiopoulos, M.L. Mangano, J. Womersley "Top Quark Physics" arXiv0003033v1

[8] Mark Thomson "Modern Particle Physics" p.189 CUP

[9] Lukas Kaj Phaf "Top Quark Production at Hadron Colliders" Geboren te Rotterdam (2014)

[10] Fabian Kohn "Measurement of the charge asymmetry in top quark pair production in pp collision data at sqrt(s) = 7 TeV using the ATLAS detector" arXiv:1204.0952

[11] NST Part III Experimental and Theoretical Physics Cambridge University, Gauge Field Theory Solutions Dr Gripaios (2014)

[12] M. Czakon, A. Mitov "Top++: a program for the calculation of the top-pair cross-section at hadron colliders" arXiv:1112.5675

[13] J.A.Benitez "Uncovering the Single Top: Observation of Electroweak Top Quark Production" Michegan State University (2009)

[14] D.Paganini "The electroweak contribution to top quark pair production: cross sections and asymmetries" arXiv1212.0808

[15] "Parton distributions for the LHC Run II" arXiv1410.8849v4

[16] NST Part II Experimental and Theoretical Physics Cambridge University, Computational Physics Using C++ Dr Richer (2014)

[17] http://mathworld.wolfram.com/MonteCarloIntegration.html

[18] http://en.wikipedia.org/wiki/Double-precision_floating-point_format

[19] http://phys.cts.nthu.edu.tw/ particle/2010TOPICAL/LHC/download /workshops_PDF/1025_1026_Pedagogical_Lectures/20101026_Lai.pdf

[20] J.Alwall, M.Herquet, F.Maltoni, O.Mattelaer, T.Stelzer arXiv1106.0522

[21] M. Czakon, A. Mitov "Inclusive Heavy Flavor Hadroproduction in NLO QCD: the Exact Analytic Result" arXiv 0811.4119v1

[22] Daniel Sherman Measurement of the Top Quark Pair Production Cross Section with $1.12fb^1$ of pp Collisions at $\sqrt{s} = 1.96TeV$" Harvard University (2007)

[23] J. Pumplin, D.R. Stump, J. Huston, H.L. Lai, P. Nadolsky, W.K. Tung arXiv 0201195v3

[24] https://www.gnu.org/software/gsl/manual/gsl-ref_24.html

[25] Werner Bernreuther (2008) "Top Quark Physics at the LHC" arxiv 0805.1333v1

[26] Jun Gao, Chong Sheng Li, Hua Xing Zhu arXiv1210.2808v3

[27] https://indico.cern.ch/event/144537/session/34/contribution/43/material/slides/0.pdf

[28] NST Part III Experimental and Theoretical Physics Cambridge University, Gauge Field Theory Notes Dr Gripaios (2014)

[29] Vera Derya "Color Factors in QCD" (2008)

[30] http://bolvan.ph.utexas.edu/ vadim/classes/2013s/qcdfr.pdf

[31] Peskin,Schroder "An Introduction to Quantum Field Theory" Westview

8 Appendix

8.1 Colour Factors

Derivations of the colour factors for the matrix elements. T^a_{ij} are the hermitian generators of the Lie Algebra of SU(3), representing colour. f^{abc} are the structure constants antisymmetric under interchange of indices, and d^{abc} are symmetric under interchange of indices. Some useful relations: [28] [29]

$$[T^a, T^b] = if^{abc}T^c \tag{25}$$

$$Tr(T^a) = 0 \tag{26}$$

$$Tr(T^aT^b) = \frac{1}{2}\delta^{ab} \tag{27}$$

$$T^aT^a = \frac{4}{3}1 \tag{28}$$

$$f^{abc}f^{abc} = 24 \tag{29}$$

$$Tr(T^aT^bT^c) = \frac{1}{4}(if^{abc} + d^{abc}) \tag{30}$$

$$
\begin{aligned}
C_{M_q^2} &= \frac{1}{9}\left|T^a_{ij}T^a_{kl}\right|^2 && \tfrac{1}{9} \text{ from averaging initial colours}\\
&= \frac{1}{9}T^a_{ij}T^a_{kl}T^b_{lk}T^b_{ji} && \text{hermicity of } T^a\\
&= \frac{1}{9}Tr(T^aT^b)Tr(T^aT^b)\\
&= \frac{1}{9}\frac{1}{4}\delta^{ab}\delta^{ab} && \text{using (27)}\\
&= \frac{2}{9}
\end{aligned}
$$

$$
\begin{aligned}
C_{M_1^2} &= \frac{1}{64}\left|T^a_{ij}T^b_{jk}\right|^2 && \tfrac{1}{64} \text{ from averaging initial gluon states}\\
&= \frac{1}{64}Tr(T^aT^bT^bT^a)\\
&= \frac{1}{64}Tr(\frac{4}{3}1\frac{4}{3}1) && \text{using (28)}\\
&= \frac{1}{12}
\end{aligned}
$$

$$
\begin{aligned}
C_{M_2^2} &= C_{M_1^2} && \text{by symmetry}\\
&= \frac{1}{12}
\end{aligned}
$$

$$
\begin{aligned}
C_{M_3^2} &= \frac{1}{64}\left|T^c_{ik}f^{abc}\right|^2 && \tfrac{1}{64} \text{ from averaging initial gluon states}\\
&= \frac{1}{64}T^c_{ik}f^{abc}f^{abd*}T^d_{ki}\\
&= \frac{1}{64}f^{abc}f^{abd}Tr(T^cT^d) && f^{abc} \text{ real, } T^a \text{ hermitian}\\
&= \frac{1}{64}\frac{1}{2}\delta^{cd}f^{abc}f^{abd} && \text{using (27)}\\
&= \frac{1}{64}\frac{1}{2}f^{abc}f^{abc}\\
&= \frac{3}{16} && \text{using (29)}
\end{aligned}
$$

$$
\begin{aligned}
C_{M_1M_2^*} &= \frac{1}{64} T^a_{ij} T^b_{jk} (T^b_{il} T^a_{lk})^* && \tfrac{1}{64} \text{ from averaging initial gluon states} \\
&= \frac{1}{64} Tr(T^a T^b T^a T^b) && \text{hermicity of } T^a \\
&= \frac{1}{64} Tr(T^a T^a T^b T^b) - i f^{abc} Tr(T^a T^c T^b) && \text{using (25)} \\
&= \frac{1}{64} (\frac{16}{3} - i f^{abc} Tr(T^a T^c T^b)) && \text{using (28)} \\
&= \frac{1}{64} (\frac{16}{3} - \frac{i}{4} f^{abc} (i f^{acb} + d^{acb})) && \text{using (29)} \\
&= \frac{1}{64} (\frac{16}{3} - \frac{1}{4} f^{abc} f^{abc}) && f^{abc} \text{ is antisymmetric, } d^{abc} \text{ symmetric} \\
&= -\frac{1}{96}
\end{aligned}
$$

$$
\begin{aligned}
C_{M_1M_3^*} &= \frac{1}{64} T^a_{ij} T^b_{jk} T^c_{ki} f^{abc} \\
&= \frac{1}{64} Tr(T^a T^b T^c) f^{abc} \\
&= \frac{1}{64} \frac{1}{4} (i f^{abc} + d^{abc}) f^{abc} && \text{using (30)} \\
&= \frac{1}{64} \frac{i}{4} f^{abc} f^{abc} && f^{abc} \text{ is antisymmetric, } d^{abc} \text{ symmetric} \\
&= \frac{3i}{32} && \text{using (29)}
\end{aligned}
$$

$$
\begin{aligned}
C_{M_2M_3^*} &= \frac{1}{64} T^b_{ij} T^a_{jk} T^c_{ki} f^{abc} \\
&= \frac{1}{64} Tr(T^b T^a T^c) f^{abc} \\
&= \frac{1}{64} \frac{1}{4} (i f^{bac} + d^{bac}) f^{abc} && \text{using (30)} \\
&= -\frac{1}{64} \frac{i}{4} f^{abc} f^{abc} && f^{abc} \text{ is antisymmetric, } d^{abc} \text{ symmetric} \\
&= -\frac{3i}{32} && \text{using (29)}
\end{aligned}
$$

8.2 Squared Matrix Elements

Derivations of the squared matrix element contributions for the $q\bar{q}$ and gg channels. Spinor indices have been suppressed for clarity. Once in the form below, these results were put in Mathematica to generate C++ code for the actual program.

Some useful relations: [28] [30] [31]

$$\gamma_\mu^\dagger = \gamma^0\gamma_\mu\gamma^0 \tag{31}$$

$$(\bar{u}(\mathbf{p}_1))^\dagger = \gamma^0 u(\mathbf{p}_1) \tag{32}$$

$$(\mathbf{p}_1+\mathbf{p}_2)^2 = \mathbf{p}_1^2+\mathbf{p}_2^2+2\mathbf{p}_1\cdot\mathbf{p}_2 = 2\mathbf{p}_1\cdot\mathbf{p}_2 \tag{33}$$

$$\sum\nolimits_P \epsilon_\mu^P(\mathbf{p})\epsilon_\nu^{*P}(\mathbf{p}) = -g_{\mu\nu} + \frac{p_\mu\bar{p}_\nu + p_\nu\bar{p}_\mu}{p\cdot\bar{p}} \equiv \Lambda_{\mu\nu} \tag{34}$$

From Section 2.3:

$$M_q = -\frac{g^2}{(\mathbf{p}_1+\mathbf{p}_2)^2}\bar{v}(\mathbf{p}_2)\gamma^\mu u(\mathbf{p}_1)\bar{u}(\mathbf{p}_3)\gamma_\mu v(\mathbf{p}_4)T_a{}^i_j T^a{}^k_l \tag{35}$$

$$\begin{aligned}
|M_q|^2 &= \frac{g^4}{(\mathbf{p}_1+\mathbf{p}_2)^4}(\bar{v}(\mathbf{p}_2)\gamma^\mu u(\mathbf{p}_1)\bar{u}(\mathbf{p}_3)\gamma_\mu v(\mathbf{p}_4))(\bar{v}(\mathbf{p}_2)\gamma^\nu u(\mathbf{p}_1)\bar{u}(\mathbf{p}_3)\gamma_\nu v(\mathbf{p}_4))^\dagger C_{M_q^2} \\
&= \frac{g^4}{(2\mathbf{p}_1\cdot\mathbf{p}_2)^2}\bar{v}(\mathbf{p}_2)\gamma^\mu u(\mathbf{p}_1)\bar{u}(\mathbf{p}_3)\gamma_\mu v(\mathbf{p}_4)\bar{v}(\mathbf{p}_4)\gamma^\nu u(\mathbf{p}_3)\bar{u}(\mathbf{p}_1)\gamma_\nu v(\mathbf{p}_1)C_{M_q^2} \\
&\qquad\qquad \text{using (31), (32) and (33)} \\
&\Rightarrow \frac{g^4}{4(2\mathbf{p}_1\cdot\mathbf{p}_2)^2}Tr[\not{p}_2\gamma^\mu\not{p}_1\gamma^\nu]Tr[(\not{p}_3+m)(1+\gamma^5\not{s}_3)\gamma_\mu(\not{p}_4-m)(1+\gamma^5\not{s}_4)\gamma_\nu]C_{M_q^2} \\
&\qquad\qquad \text{averaging over initial spins and using spin relations (12) and (13)}
\end{aligned}$$

Again, from section 2.3:

$$M_1 = -\frac{g^2}{2(\mathbf{p}_1\cdot\mathbf{p}_3)}\bar{u}(\mathbf{p}_3)\gamma^\mu(\not{p}_3-\not{p}_1+m)\gamma^\nu v(\mathbf{p}_4)\epsilon_\mu(\mathbf{p}_1)\epsilon_\nu(\mathbf{p}_2)T_a{}^i_j T^b{}^j_k \tag{36}$$

$$M_2 = -\frac{g^2}{2(\mathbf{p}_2\cdot\mathbf{p}_3)}\bar{u}(\mathbf{p}_3)\gamma^\nu(\not{p}_3-\not{p}_2+m)\gamma^\mu v(\mathbf{p}_4)\epsilon_\mu(\mathbf{p}_1)\epsilon_\nu(\mathbf{p}_2)T_b{}^i_j T^a{}^j_k \tag{37}$$

$$M_3 = \frac{ig^2}{(\mathbf{p}_1+\mathbf{p}_2)^2}\bar{u}(\mathbf{p}_3)\gamma^\rho v(\mathbf{p}_4)\epsilon_\mu(\mathbf{p}_1)\epsilon_\nu(\mathbf{p}_2)V_{\mu\nu\rho}T_c{}^i_k f^{abc} \tag{38}$$

$$V_{\mu\nu\rho} = (\mathbf{p}_1-\mathbf{p}_2)_\rho g_{\mu\nu} + (2\mathbf{p}_2+\mathbf{p}_1)_\mu g_{\nu\rho} - (2\mathbf{p}_1+\mathbf{p}_2)_\nu g_{\mu\rho} \tag{39}$$

$$|M_1|^2 = \frac{g^4}{(2\mathbf{p}_1\cdot\mathbf{p}_3)^2}(\bar{u}(\mathbf{p}_3)\gamma^\mu(\not{p}_3-\not{p}_1+m)\gamma^\nu v(\mathbf{p}_4))(\bar{u}(\mathbf{p}_3)\gamma^\alpha(\not{p}_3-\not{p}_1+m)\gamma^\beta v(\mathbf{p}_4))^\dagger$$
$$|\epsilon_\mu(\mathbf{p}_1)\epsilon_\nu(\mathbf{p}_2)|^2 C_{M_1^2}$$
$$= \frac{g^4}{(2\mathbf{p}_1\cdot\mathbf{p}_3)^2}(\bar{u}(\mathbf{p}_3)\gamma^\mu(\not{p}_3-\not{p}_1+m)\gamma^\nu v(\mathbf{p}_4))(\bar{v}(\mathbf{p}_4)\gamma^\beta(\not{p}_3-\not{p}_1+m)\gamma^\alpha u(\mathbf{p}_3))$$
$$|\epsilon_\mu(\mathbf{p}_1)\epsilon_\nu(\mathbf{p}_2)|^2 C_{M_1^2}$$
using (31),(32) and (33)
$$\Rightarrow \frac{g^4}{4(2\mathbf{p}_1\cdot\mathbf{p}_3)^2}Tr[(\not{p}_3+m)(1+\gamma^5\not{\epsilon}_3)\gamma^\mu(\not{p}_3-\not{p}_1+m)\gamma^\nu(\not{p}_4-m)(1+\gamma^5\not{\epsilon}_4)$$
$$\gamma^\beta(\not{p}_3-p_1+m)\gamma^\alpha]\Lambda_{\mu\alpha}\Lambda_{\nu\beta}C_{M_1^2}$$
averaging gluon polarisations and using (12),(13) and (34)

$$|M_2|^2 = \frac{g^4}{4(2\mathbf{p}_2\cdot\mathbf{p}_3)^2}Tr[(\not{p}_3+m)(1+\gamma^5\not{\epsilon}_3)\gamma^\nu(\not{p}_3-\not{p}_2+m)\gamma^\mu(\not{p}_4-m)(1+\gamma^5\not{\epsilon}_4)$$
$$\gamma^\alpha(\not{p}_3-p_2+m)\gamma^\beta]\Lambda_{\mu\alpha}\Lambda_{\nu\beta}C_{M_2^2}$$
same as $|M_1|^2$ but with $\mathbf{p}_1 \leftrightarrow \mathbf{p}_2$ and $\mu \leftrightarrow \nu$

$$|M_3|^2 = \frac{g^4}{((\mathbf{p}_1+\mathbf{p}_2)^4}(\bar{u}(\mathbf{p}_3)\gamma^\rho v(\mathbf{p}_4))(\bar{u}(\mathbf{p}_3)\gamma^\sigma v(\mathbf{p}_4))^\dagger V_{\mu\nu\rho}V^*_{\alpha\beta\sigma}\,|\epsilon^\mu(\mathbf{p}_1)\epsilon^\nu(\mathbf{p}_2)|^2 C_{M_3^2}$$
$$\Rightarrow \frac{g^4}{4(2\mathbf{p}_1\cdot\mathbf{p}_3)^2}Tr[(\not{p}_3+m)(1+\gamma^5\not{\epsilon}_3)\gamma^\rho(\not{p}_4-m)(1+\gamma^5\not{\epsilon}_4)\gamma^\sigma]V_{\mu\nu\rho}V_{\alpha\beta\sigma}\Lambda_{\mu\alpha}\Lambda_{\nu\beta}C_{M_3^2}$$
averaging gluon polarisations and using (12)(13), (31)-(34), and the fact V is real

$$M_1 M_2^* = \frac{g^4}{4(\mathbf{p}_1\cdot\mathbf{p}_3)(\mathbf{p}_2\cdot\mathbf{p}_3)}(\bar{u}(\mathbf{p}_3)\gamma^\mu(\not{p}_3-\not{p}_1+m)\gamma^\nu v(\mathbf{p}_4))(\bar{u}(\mathbf{p}_3)\gamma^\beta(\not{p}_3-\not{p}_2+m)\gamma^\alpha v(\mathbf{p}_4))^\dagger$$
$$|\epsilon_\mu(\mathbf{p}_1)\epsilon_\nu(\mathbf{p}_2)|^2 C_{M_1M_2^*}$$
$$= \frac{g^4}{4(\mathbf{p}_1\cdot\mathbf{p}_3)(\mathbf{p}_2\cdot\mathbf{p}_3)}\bar{u}(\mathbf{p}_3)\gamma^\mu(\not{p}_3-\not{p}_1+m)\gamma^\nu v(\mathbf{p}_4)\bar{v}(\mathbf{p}_4)\gamma^\alpha(\not{p}_3-\not{p}_2+m)\gamma^\beta u(\mathbf{p}_3)$$
$$|\epsilon_\mu(\mathbf{p}_1)\epsilon_\nu(\mathbf{p}_2)|^2 C_{M_1M_2^*}$$
using (31),(32) and (33)
$$\Rightarrow \frac{g^4}{16(\mathbf{p}_1\cdot\mathbf{p}_3)(\mathbf{p}_2\cdot\mathbf{p}_3)}Tr[(\not{p}_3+m)(1+\gamma^5\not{\epsilon}_3)\gamma^\mu(\not{p}_3-\not{p}_1+m)\gamma^\nu(\not{p}_4-m)(1+\gamma^5\not{\epsilon}_4)$$
$$\gamma^\alpha(\not{p}_3-p_2+m)\gamma^\beta]\Lambda_{\mu\alpha}\Lambda_{\nu\beta}C_{M_3^2}C_{M_1M_2^*}$$
averaging gluon polarisations and using (12),(13) and (34)

$$M_1 M_3^* = \frac{ig^4}{4(\mathbf{p}_1\cdot\mathbf{p}_2)(\mathbf{p}_1\cdot\mathbf{p}_3)}(\bar{u}(\mathbf{p}_3)\gamma^\mu(\not{p}_3-\not{p}_1+m)\gamma^\nu v(\mathbf{p}_4))(\bar{u}(\mathbf{p}_3)\gamma^\rho v(\mathbf{p}_4))^\dagger$$
$$V^*_{\alpha\beta\rho}|\epsilon_\mu(\mathbf{p}_1)\epsilon_\nu(\mathbf{p}_2)|^2 C_{M_1M_3^*}$$
$$= \frac{ig^4}{4(\mathbf{p}_1\cdot\mathbf{p}_2)(\mathbf{p}_1\cdot\mathbf{p}_3)}\bar{u}(\mathbf{p}_3)\gamma^\mu(\not{p}_3-\not{p}_1+m)\gamma^\nu v(\mathbf{p}_4)(\bar{v}(\mathbf{p}_4)\gamma^\rho u(\mathbf{p}_3)$$
$$V_{\alpha\beta\rho}|\epsilon_\mu(\mathbf{p}_1)\epsilon_\nu(\mathbf{p}_2)|^2 C_{M_1M_3^*}$$
using (31) and (32), and fact V is real
$$\Rightarrow \frac{ig^4}{16(\mathbf{p}_1\cdot\mathbf{p}_2)(\mathbf{p}_1\cdot\mathbf{p}_3)}Tr[(\not{p}_3+m)(1+\gamma^5\not{\epsilon}_3)\gamma^\mu(\not{p}_3-\not{p}_1+m)\gamma^\nu(\not{p}_4-m)$$
$$(1+\gamma^5\not{\epsilon}_4)\gamma^\rho]V_{\alpha\beta\rho}\Lambda^\alpha_\mu\Lambda^\beta_\nu C_{M_1M_3^*}$$
averaging gluon polarisations and using (12),(13) and (34)

$$M_2 M_3^* = \frac{ig^4}{16(\mathbf{p}_1\cdot\mathbf{p}_2)(\mathbf{p}_2\cdot\mathbf{p}_3)}Tr[(\not{p}_3+m)(1+\gamma^5\not{\epsilon}_3)\gamma^\nu(\not{p}_3-\not{p}_2+m)\gamma^\mu(\not{p}_4-m)$$
$$(1+\gamma^5\not{\epsilon}_4)\gamma^\rho]V_{\alpha\beta\rho}\Lambda^\alpha_\mu\Lambda^\beta_\nu C_{M_1M_3^*}$$
same as $M_1M_2^*$, but with $\mathbf{p}_1\leftrightarrow\mathbf{p}_2$ and $\mu\leftrightarrow\nu$